Activity reports of the Italian CRG beamline at the European Synchrotron Radiation Facility (ESRF)

Grenoble, December 2015

Responsabile editoriale: Francesco d'Acapito (*dacapito@iom.cnr.it*)

Editing: Roberta De Donatis (*roberta.dedonatis@cnr.it*)

ISSN: 2465-1346

LISA

Annual Report 2015

N. 3 - December 2015

Istituto Officina dei Materiali

Abstract

This document summarizes the activity of the italian CRG beamline at ESRF (LISA project) during year 2015. Statistic data on the beamline use are presented as well as the latest major instrumental advancements, highlight experiments and publications.

Keywords

Italian beamline at ESRF, BM08

LISA project

X-ray Absorption Spectroscopy

Index

2015 has been the first year of official activity of the LISA project. The financial contribution from CNR has been received and the campaign for the procurement of the new optical elements has started.

After a call for proposals and a poll process among users, LISA has a logo, as you can see in the side picture. Feel free to use it for your posters and presentations concerning data collected at the beamline.

The official logo of the LISA beamline

LISA has also a new staff with Dr. Alessandro Puri and Dr. Giovanni Lepore that have started their activity at the beamline during this year. Alessandro comes from the High Field Magnet Laboratory in Nijmegen and has competences in magnetic materials. Giovanni comes from the department of Earth Science of the Florence University and has competences in crystallography. A warm goodbye to Angela Trapananti who left the group in Grenoble for Perugia and who will continue her collaboration with LISA as a highly skilled user.

CNR has also appointed a new Beamtime review panel for the Italian quota that will be operative till 2019.

During 2015 LISA has delivered 377 shifts to ESRF and CRG users with no significant problems on the instrumentation and 23 experiments have been carried out. A noticeable amount of beamtime has been dedicated to the formation of the new staff (that is at present fully operative) and to the implementation of new instrumentation and data collection modes as reported in the following sections. Concerning the formation activity, LISA has continued the participation to the HERCULES international school with the practical lectures on XAS and three students from Italian universities have been hosted at the beamline for stages on data collection and analysis: Irene Carrasco, from Verona, Chiara Petroselli from Perugia and Stefano Pelli Cresi from Bologna.

25 publications related to works carried out at LISA have been published in 2015 accordingly to the ESRF-ILL joint library site (data at Dec 2015).

Work in progress

The refurbishment of the beamline consists in the renewal of the X-ray optics and adaptation of the existing infrastructures.

For the first part CINEL company has won the selection for the production of the new monochromator whereas the Call for Tender for the mirrors will be launched at the end of the year. The monochromator will have two crystal pairs for energy selection [Si(311) and Si(111)] and will be operative in the range 4-72 keV. It will use flat thick crystals and will be cooled with liquid nitrogen.

The roadmap of the interventions for the renewal of the infrastructures has been defined with the ESRF technical services, under the supervision of Eric Dettona of the CRG Liaison group of ESRF. The new experimental hutch has been created with the removal of the wall that divided the former GILDA's diffraction and third hutches. During the summer shutdown in 2016 the electrical distribution will be totally rebuilt and this will have just a moderate impact on the users activity.

Picture of the new experimental hutch of Lisa

During year 2016 the liquid nitrogen line (for the monochromator cooling) will be realized. The installation of the optical elements in the optic hutch and commissioning is foreseen at present for spring 2017. In the second half of 2017 LISA will accept users with the new instrumentation.

Microtomo furnace

The LISA beamline is now configured to work with the microtomo furnace available from the instrument pool. This furnace is extremely compact and can be mounted directly inside the EXAFS chamber in both absorption and fluorescence modes. The system allows full temperature control between room temperature and 800 °C both under vacuum and gas flow, allowing in-situ measurements during temperature annealing or chemical reactions.

The temperature is settled via Eurotherm controller, which allows maximum ramping rate of 10°C/min and really good thermal stability. It's also possible to program a thermal cycle.

At the moment remote control is not possible and the target temperature needs to be entered manually, work is in progress to integrate the temperature control in SPEC. Test are also in progress to operate the microtomo together with a mass spectrometer for the analysis of the reaction gases.

Left: view of the cell with the control electronics.
Right: detail of the cell without the cover dome.

Pump and probe stroboscopic studies

In 2015 important improvements have been achieved in the field of time resolved studies thanks to the procurement of a high-current driver for the Ultra-Violet LED. The prototype, realized by AGE-Scientific/CAEN, permits to send short pulses with high current in the LED. The maximum current is 1.5 A whereas the minimum pulse duration is about 50ns, limited by the internal capacitance of the diode. This device permits the realization of pump-and-probe experiments in stroboscopic mode with the storage ring operating in 4 bunches (4b) mode, when the spacing between the X-ray pulses is about 700 ns. Test experiments have been carried out (in collaboration with the chemical departments of the Milano and Pavia universities, A. Minguzzi and P. Ghigna) on a system consisting in an electrochemical cell with a photoanode of hematite-Iridium oxide. The XAS experiment was carried out at the Ir-L_{III} edge and light at 400nm from the LED was sent, through a focusing optics, to the photoanode with the cell at different potential values. The study aimed to evidence the charge transfer between Ir and hematite upon UV photon absorption by the iron oxide.

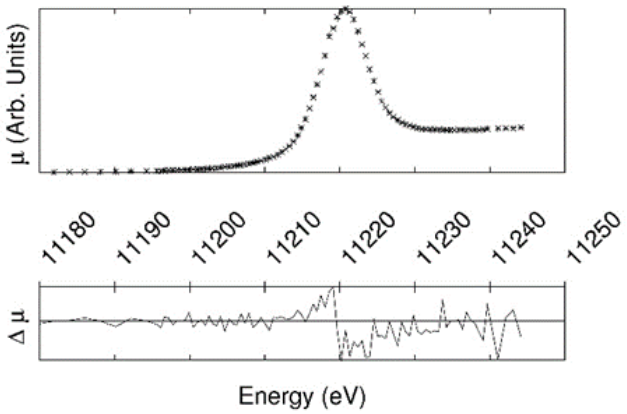

Upper panel: spectra of the photoanode with and without pump (UV light, 600ns from the probe). Lower panel: difference spectrum.

In the picture on the left the response of the system (with the cell at a potential of 1.46V vs the Reversible Hydrogen Electrode) to the LED illumination is presented. In the upper panel there are two spectra collected with and without light. The differences are extremely small and they can only be evidenced showing the difference spectra. In the lower panel the differences between pump/no-pump spectra are shown in the case of a pump-probe delay value of 600 ns.

This demonstrates the capability of the system to realize XAS experiments in stroboscopic mode. For the future it is foreseen the procurement of a LED more adapted to fast pulses or of a laser diode In order to obtain pulses of a few ns of duration.

Advances in the XEOL apparatus

The apparatus for the collection of XEOL data was improved with the availability of bandpass filters for the wavelength selection and the use of a suitable time-controllable gate for the PMT (Photo Multiplier Tube) detector pulses. This permitted the realization of experiments resolved in wavelength and time. Data shown hereafter come from an experiment carried out with the ring operating in 16 bunch mode, with the X-ray pulses separated by 180 ns. The sample was a pellet of Zinc Oxide (ZnO) which is known to emit under X-ray excitation (Armelao et al. J Phys. Chem C 2007, 111 ,10194) in two bands one centered at 390 nm (gap transition) and the other at 500nm (defect states).

XAS data were collected at the Zn-K edge, the sample luminescence was collected by a lens and sent, via an optic fiber, to a fast Photomultiplier with the possibility of inserting a bandpass filter (FWHM = 10nm) for wavelength selection. The results are shown in the pictures below:

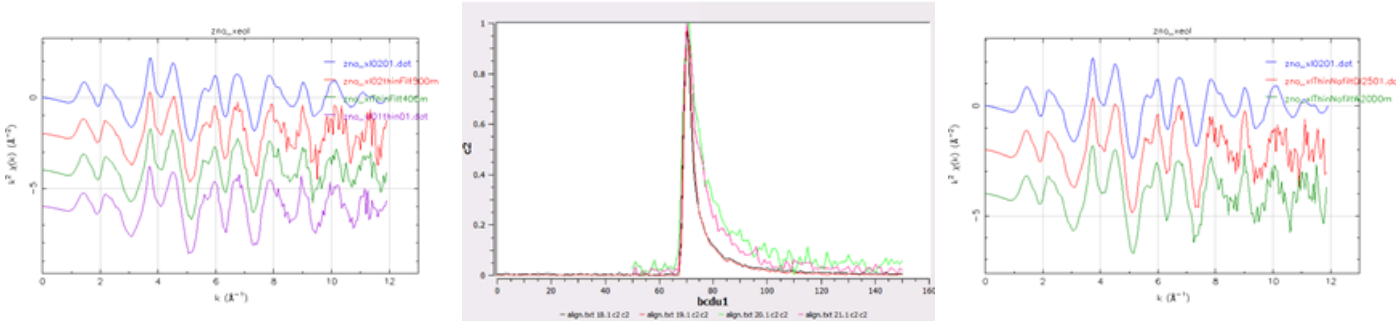

Left: XEOL-XAS data collected at different emission wavelength. Center: Time response of XEOL at different wavelengths. Right: XEOL-XAS spectra collected at different times after the X-ray pulse. (see text for details)

The plot in the left side shows spectra taken at different wavelength values (purple: full emission, green: 400nm, red 500nm) compared with the data taken in transmission mode (blue line). In all cases a signal of good quality could be collected demonstrating the effectiveness of the use of bandpass filters for wavelength-resolved XEOL.

The plots in the center and right panels refer to time-resolved data collection. The central panel shows the emission from the sample for different values of delay between the x-ray flash (arriving at about 70ns in the time abscissa) and the position of the pulse collection window (width=10ns); data were adapted to a common scale for an easier comparison. The decay of the curve is linked to the decay of the luminescence at the selected wavelength. Data were collected for the full emission (Black curve), emission at 400nm (red), 450nm (pink), 500nm (green): as expected, the emission at longer wavelength is slower.

The right panel presents XEOL data collected using the full emission but selecting the arrival time of the pulses from the PMT in coincidence with the X flashes (red curve) or in the window 90-150 ns after the X (green curve) compared with the spectrum in transmission mode. Also in this case the data quality is sufficient for the collection of XAS data.

SDD detector

The Lisa beamline is now configured to work with SDD detector available from the instrument pool. This type of detectors offers two advantages: It has a high dynamic range which is useful when you need to detect fluorescence signals in samples embedded in a matrix with a large unwanted background. Moreover the detector is very compact and can be placed really close the sample to maximize the signal.

Left: view of the detector and readout electronics.
Right: close-up of the detector

The resistive switching mechanism of Conductive Bridging Random Access Memories clarified by using synchrotron characterizations

E. Souchier,[‡ab], F. d'Acapito,[c], P. Noé,[ab], P. Blaise,[ab], M. Bernard[ab] and V. Jousseaume[ab]

[a] Univ. Grenoble-Alpes, France, [b] CEA-LETI-MINATEC, France, [c] CNR-IOM-OGG c/o ESRF France,
[‡] Present address: Dolphin Integration/IBM

In recent years, resistive random access memories have received extensive interest for applications as non-volatile memories or neuromorphic computing. Conductive Bridging Random Access Memories (CBRAM) based on a glassy Ag-GeSx layer sandwiched between an Ag anode and an inert W cathode are considered to be one of the most promising technologies. Under the influence of an electric field Ag ions are produced at the anode and migrate in the electrolyte reaching the cathode and forming a conducting wire. This process is reversible by applying a bias with opposite polarity. However, the lack of understanding of the switching mechanisms at a nanoscale level prevents the successful transfer of this technology to the industry.
CBRAM devices were characterized in their different resistive states using depth-selective X-Ray Absorption Spectroscopy (XAS). Figure (a) presents the XAS spectra depending on the switching state of the device and on the depth. As-deposited CBRAMs shows a lower silver metal fraction with respect to the switched ones. Moreover, XAS surface data show a higher metal fraction below the anode with respect to the entire layer. Our experiments highlight that the switching process involves the formation of metallic Ag cone-shaped nanofilaments with their base on the active electrode. Moreover, the study reveals that Ag is in two very distinct environments with short Ag-S bonds due to Ag dissolved in the GeSx matrix and longer Ag-Ag bonds related to an Ag metallic phase. Ab initio molecular dynamics (MD) simulations confirm that Ag favorably binds to S atoms. This provides an explanation on the reported instability of the ON state that can be attributed to Ag sulphidation and hence a rupture of the Ag–Ag metallic conduction path in the stack.

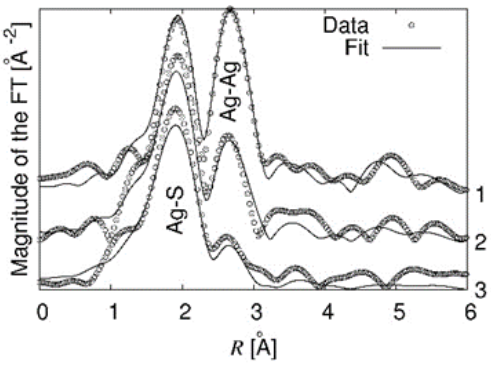

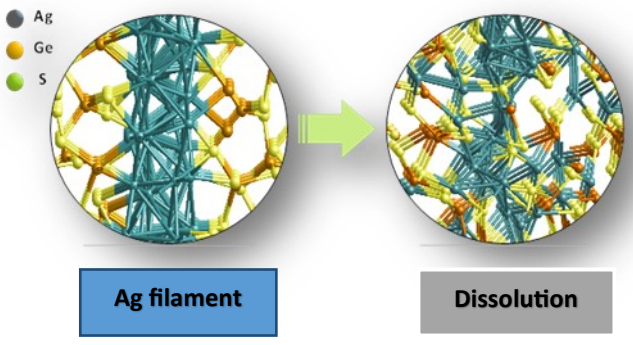

Left: Fourier Transforms of XAS spectra of 3 prototypical samples: 1=switched CBRAM at the surface, below the anode 2= switched CBRAM in the whole layer, 3=pristine CBRAM at the surface.
Right: Schematic of a silver nano-filament in Ag–GeSx and the silver filament dissolution as obtained by MD.

Publication: E. Souchier et al., Phys. Chem. Chem. Phys. 17 (2015) 23931.

Structural modifications in ceria-supported silver nanoparticles

F. Benedetti[1,2], P. Luches[2], M. C. Spadaro[1,2], G. Gasperi,[1,2], S. D'Addato[1,2], S. Valeri[1,2], F. Boscherini[3,4]

[1]Univ. of Modena and Reggio Emilia, Italy, [2]CNR-NANO, Modena, Italy [3]Univ. of Bologna, Italy, [4]CNR-IOM, France.

The Ag/cerium oxide system is gaining an increasing importance in catalytic applications, showing a higher activity and durability than its individual components. An atomic scale insight into the structure of Ag nanoparticles supported on CeO_2 and of the metal/oxide interface is of great help to fully understand and optimize the properties of the system.

Highly-diluted samples made of Ag particles of different size in the nm range, supported on well-defined cerium oxide (111) surfaces (Fig.1), were investigated by X-ray absorption fine structure at the Ag K-edge, in the near and extended energy range in different scattering geometries. The data analysis showed that the nanoparticles have the face centered cubic structure with an Ag−Ag interatomic distance contracted by 3−4% with respect to the bulk value, due to dimensionality induced effects (Fig.2). The Ag−O interfacial interatomic distance was found to decrease with decreasing nanoparticle size, evidencing a stronger interaction with the oxide as the nanoparticle size becomes smaller.

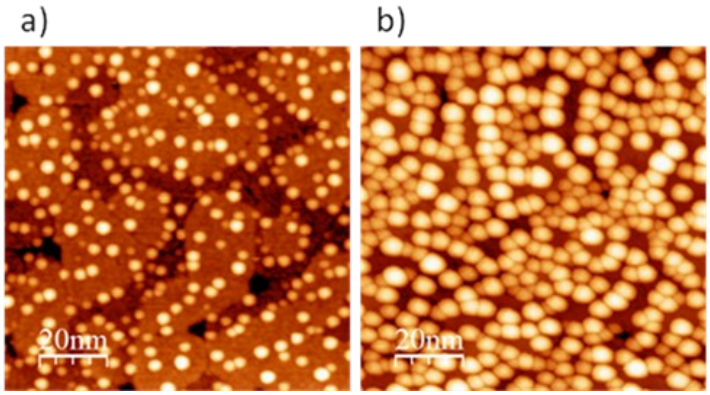

Fig. 1: STM images of Ag nanoparticles obtained by growing (a) 0.2 Å Ag and (b) 1.5 Å Ag on 10 ML thick (111) oriented CeO_2 films.

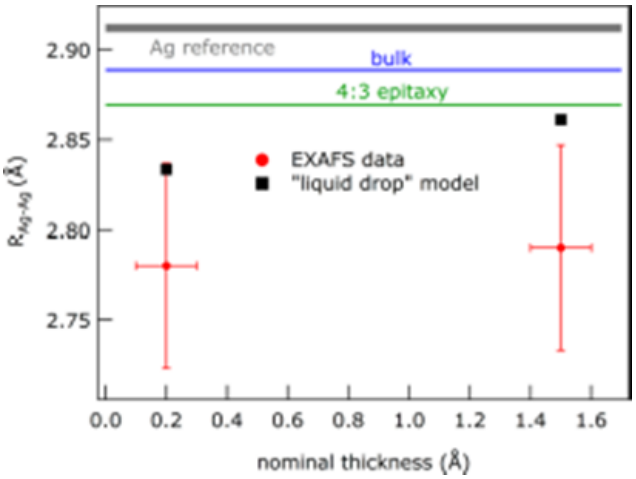

Fig. 2: Ag−Ag interatomic distance for the 0.2 Å Ag and 1.5 Å Ag samples on CeO2 obtained from the EXAFS analysis. The thick grey line is the value measured on the metallic reference sample. The green line is the value expected assuming an epitaxial contraction of 0.7%. The black squares represent the values obtained for the dimensionality-related contraction using the "liquid drop" model.

Publication: F. Benedetti et al. J. Phys. Chem. C 119 (2015) 6024.

Defects related to metal substitution: Fe and Co in ZnO nanoparticles

G. Giuli,[$] A. Trapananti,[#] F. Mueller,[†, §,‡] D. Bresser,[†, §] F. d'Acapito,[#] S. Passerini [†, §]

[$]Univ Camerino, Italy, [#]CNR- IOM-OGG, c/o ESRF, France [†]Helmholtz Institute Ulm, Germany
[§]Karlsruhe Institute of Technology, Germany, [‡]Univ. of Muenster Germany

Synthesis of metal oxide solid solution with a controllable defect chemistry and defect concentration could be of fundamental importance in order to tailor the physical properties of oxide material. Herein, we report an in depth structural study of Fe- and Co-doped ZnO nanopowders by using X-ray Absorption Spectroscopy (XAS), to study the influence of the dopant on the crystallite structure, the effective incorporation of the dopant in the host lattice and to investigate the major differences between Co- and Fe-doped ZnO nanoparticles regarding the dopant oxidation state and the presence of local defects such as cationic vacancies or anionic interstitials caused by the substitution.

XAS of Co- and Fe- doped ZnO nanoparticles reveal the effective incorporation of such transition metal dopants into the host material without formation of metallic nanoclusters or additional oxide phases. Both dopants, are located in the tetrahedral sites of the ZnO lattice substituting for Zn. No significant fractions of both Fe and Co were found in the interstitial sites. Near Edge (XANES) data clearly reveal that Co is divalent whereas Fe is mostly trivalent in the investigated samples. The presence of Fe^{3+} (substituting for Zn^{2+}) implies the existence of charge compensating local defects in the structure (such as cationic vacancies or interstitial oxygen). This hypothesis is supported by the EXAFS data: while at the Co K-edge there is a clear contribution to the EXAFS signal associated with the Co-Zn second coordination shell, similarly to the Zn K-edge signals, the corresponding signal is strongly damped at the Fe K-edge (Fig. 1, right panel). This intensity reduction may be attributed to the occurrence of local defects triggered by the presence of trivalent Fe^{3+} such as Zn vacancies or interstitial oxygen ions.

The results of this study are of substantial importance to unfold the (de-) lithiation mechanism in general as well as in dependence on the incorporated dopant. We propose that the different oxidation state of the Fe and Co dopant is reflected in the different shape of the recorded potential profiles of such materials, indicating a slightly different (initial) lithiation reaction during cycling. In addition, we assume that the absence of metallic TM nano-phases in the pristine material enables the excellent reversibility of the Li_2O formation during cycling.

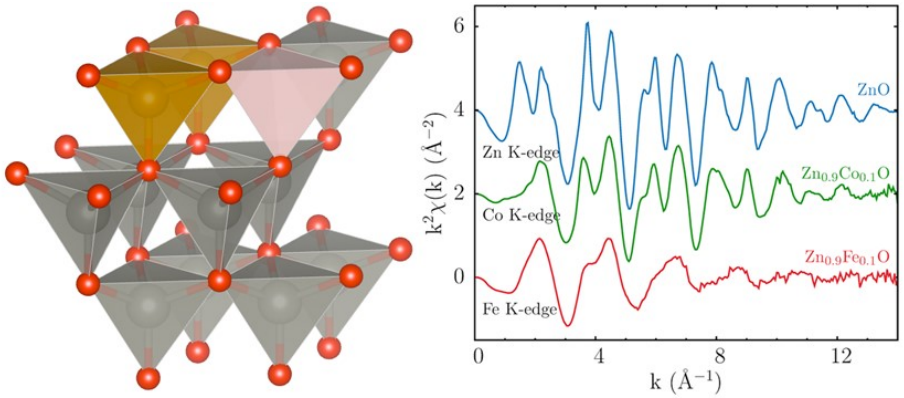

Figure 1, Left: Sketch of the ZnO structure (gray Zn and red O) with a hypotetical FeO_4 dimer (orange) coupled with a charge compensating Zn vacancy (pink). Right: comparison of the experimental Zn-, Co - and Fe- K-edge EXAFS spectra revealing oscillations of reduced amplitude at the Fe K-edge. This reduced amplitude is compatible with both the presence of cationic vacancies and/or the presence of interstitial oxygen.

Publication: G. Giuli et al. Inorg. Chem. 54 (2015), 9393-9400.

Easy Accommodation of Different Oxidation States in Iridium Oxide Nanoparticles With Different Hydration Degree as Water Oxidation Electrocatalysts

A. Minguzzi[*1,2], C. Locatelli[1,2], O. Lugaresi[1,§], E. Achilli[3], G. Cappelletti[1], M. Scavini[2,4], M. Coduri[1,5], P. Masala[1], B. Sacchi[1], A. Vertova[1,2,4], P. Ghigna[2,3], S. Rondinini[1,2,4]

[1]Univ. Milano, [2]INSTM, [3]Univ. Pavia, [4]CNR- ISTM, [5]CNR, - IENI, [§]now at Mettler-Toledo S.p.A.

Iridium oxide represents one of the most active electrocatalyst for the oxygen evolution reaction, the process that limits the kinetics of water electrolysis for high purity H_2 production. Understanding the mechanism of action of the Ir active sites is thus needed for the design of catalysts with lower costs. In a previous work [Chem. Sci. 5 (2014) 3591] we observed by *in-operando* XANES on hydrous, electrodeposited IrO_x the presence of Ir(III) and Ir(V) at potentials at which oxygen was evolved. However, the low stability of this amorphous material might not represent a good model for materials used at the industrial level. For this reason we focused our attention on crystalline IrO_2 prepared on an Ir core thus having a high percentage of surface Ir-O and allowing the use of *in-operando* XAS. Thanks to this strategy we confirmed the existence of the two oxidation states assumed by Ir during the catalytic cycle (Figure 1).

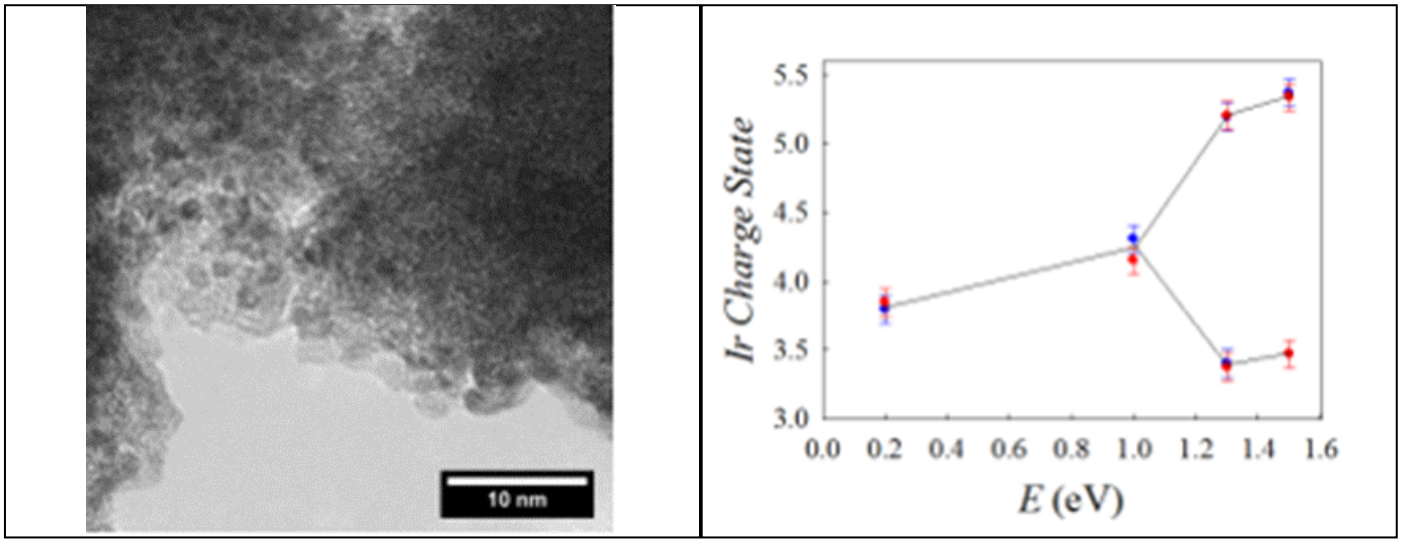

Figure 1, Left: an high resolution TEM image of the IrO2/Ir powder. Right: Dependence on the Ir charge state on the applied potential, obtained according to the Ir-LIII edge XANES peak thanks to the comparison with Ir(III) and Ir(IV) standards

Moreover, the EXAFS analysis evidenced a negligible variation of the Ir-O length in the whole considered potential window, suggesting that IrO_2 is capable of accomodating different oxidation states without a significant structure change. This likely represents one of the reasons behind the exceptional activity of this material.

Publication: A. Minguzzi et al. ACS Cat. 5 (2015), 5104.

The chemical environment of iron in mineral fibres. A combined X-ray absorption and Mössbauer spectroscopic study

S. Pollastri,[a] F. d'Acapito,[b] A. Trapananti,[b] I. Colantoni,[c] G.B. Andreozzi,[d] A.F. Gualtieri[a]

[a]Univ. of Modena and Reggio Emilia, Italy; [b]CNR-IOM-OGG c/o ESRF, France;
[c]Univ. Rome "Tor Vergata", Italy; [d]Univ. Rome "La Sapienza", Italy.

Although asbestos represents today one of the most harmful contaminant on Earth, in 72% of the countries worldwide only amphiboles are banned while controlled use of chrysotile is allowed. Uncertainty on the potential toxicity of chrysotile is due to the fact that the mechanisms by which mineral fibres induces cyto- and geno-toxic damage is still unclear. We have recently started a long term project aimed at the systematic investigation of the crystal-chemistry, bio-interaction and toxicity of the mineral fibres. This work presents a systematic structural investigation of iron in asbestos and erionite (considered the most relevant mineral fibres of social and/or economic-industrial importance) using synchrotron X-ray absorption and Mössbauer spectroscopy. In all investigated mineral fibres, iron in the bulk structure is found in octahedral sites (Fig. 1) and can be made available at the surface via fibre dissolution. We postulate that the amount of hydroxyl radicals released by the fibers depends, among other factors, upon their dissolution rate; in relation to this, a ranking of ability of asbestos fibres to generate hydroxyl radicals, resulting from available surface iron, is advanced: amosite > crocidolite ≈ chrysotile > anthophyllite > tremolite. Erionite, with a fairly high toxicity potential, contains only octahedrally coordinated Fe^{3+}. Although it needs further experimental evidence, such available surface iron may be present as oxide nanoparticles coating and can be a direct cause of generation of hydroxyl radicals.

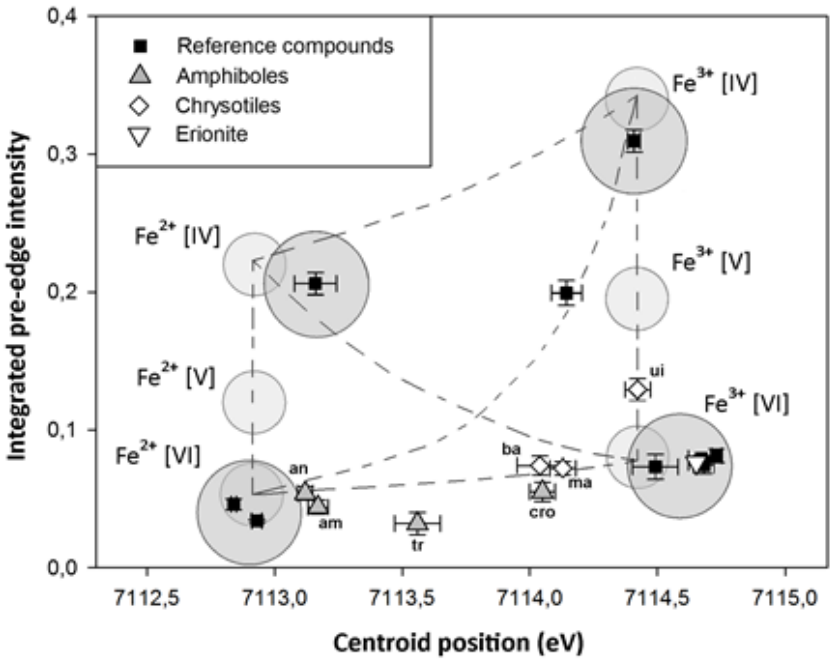

Figure 1:
Pre-edge parameters of samples and reference compounds plotted in the modified variogram from [Wilke et al. 2005]. Little grey fields designate pre-edge parameters for the Fe coordination and oxidation state whereas dashed lines between fields indicate the variation of pre-edge parameters assuming binary mixtures of respective end-members. Darker grey fields designate our pre-edge parameter.

Publication: S. Pollastri et al. J. Haz. Mat. 298 (2015) 282.

The effect of the [Na/(Na+K)] ratio on Fe speciation in phonolitic glasses

M.R. Cicconi[1,2], G. Giuli[2], W. Ertel-Ingrisch[3], E. Paris[2], D.B. Dingwell[3]

[1]FAU Erlangen-Nürnberg, Germany, [2]Univ. Camerino, Italy, [3]LMU Munich, Germany

Natural iron-bearing alkali-rich phonolitic melts represent an extreme compositional range of the effect of the [Na/(Na+K)] ratio on the Fe geochemical behavior in volcanic systems. Unfortunately, with the exception of data available for basaltic, andesitic and simplified ferrosilicate melts, the effect of iron redox state on alkali rich phonolitic melts still needs to be assessed. Fe *K*-edge XAS spectra have been used to constrain the Fe structural role (oxidation state, coordination number, bond distances) in phonolitic glasses as a function of temperature (*T*), [Na/(Na+K)] ratio (= 0.0, 0.25, 0.5, 0.75, 1.0) and redox state. We verified that different [Na/(Na+K)] ratios strongly affect the $Fe^{3+}/(Fe^{2+}+Fe^{3+})$ ratio for any oxygen fugacity conditions: in particular, the Fe redox ratio decreases by increasing the [Na/(Na+K)] ratio. This behavior suggests that Fe^{3+} is stabilized by cations with lower ionic potential and prefers the 4-fold coordination when sufficient alkalis are available for charge balance. Therefore, Fe^{3+} behaves as a structural analogous of Al3+. EXAFS analysis confirms that Fe3+ is 4-fold coordinated with <Fe-O> distance of 1.88 ± 0.02 Å, in agreement with previous studies. The deviation between experimental data and theoretical estimations confirms that current thermodynamical models are still not able to reproduce the magnitude of the variations of the Fe redox ratio when changing relevant parameters, such as T and alkali ratio.

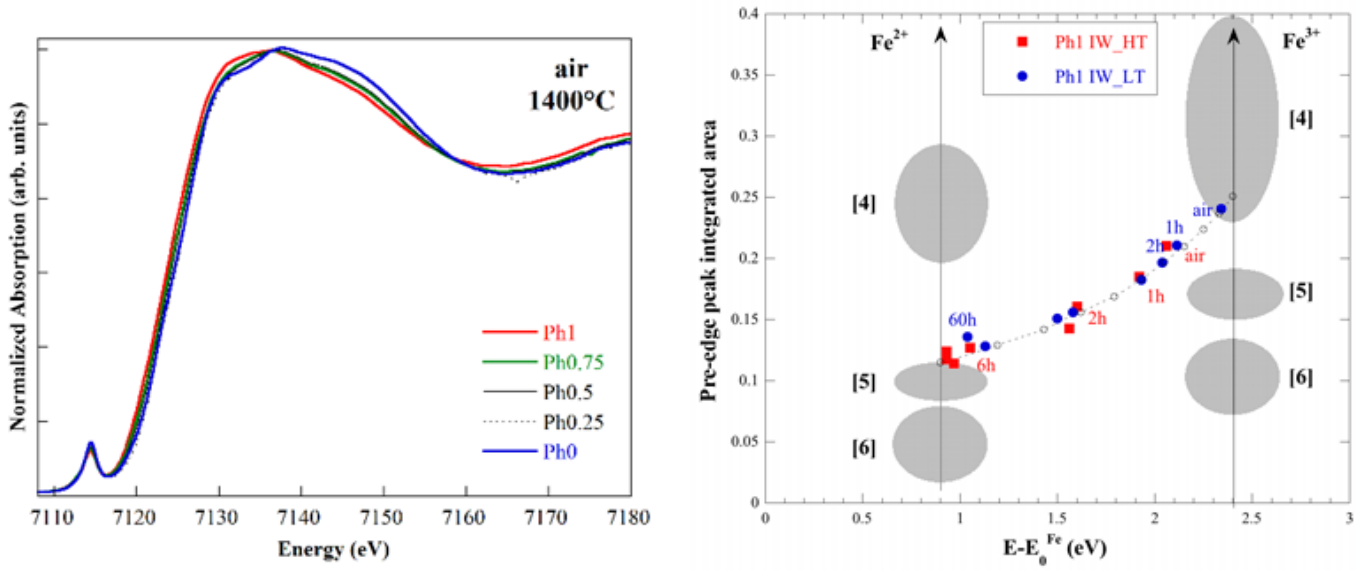

Figure 1, Left: XAS spectra of the five glasses synthesized in air at high temperature. In the edge region is evident a shift toward lower energies corresponding to the increase of the [Na/(Na+K)] ratio. Right: Plot of the pre-edge peak integrated area vs. centroid position for the kinetic experiments of glass Ph1 done at higher and lower temperatures (HT and LT, respectively). The evolution of the redox for different times is clearly different for the two different synthesis temperatures.

Publication: M. R. Cicconi et al. Amer. Min. 100 (2015), 1610.

Cu(I) binding to monomeric α and β synuclein

R. De Ricco[1,2], D. Valensin[1], S. Dell'Acqua[2], L. Casella[2], S. Mangani[1]

[1]Univ. Siena Italy, [2]Univ. Pavia, Italy

Parkinson's disease (PD) is a neurodegenerative disorder characterized by the presence of abnormal α-synuclein (αS) deposits in the brain. Alterations in homeostasis and metal-induced oxidative stress may play a crucial role in the progression of αS amyloid assembly and pathogenesis of PD. Contrary to αS, β-synuclein (βS) is not involved in the PD etiology. However, it has been suggested that the βS/αS ratio is altered in PD, indicating that a correct balance of these two proteins is implicated in the inhibition of αS aggregation. αS and βS share similar abilities to coordinate Cu(II), but they also bind Cu(I) ions. Cu(II) and Cu(I) ions are implicated in PD since they accelerate the aggregation process and they are involved in the production of reactive oxygen species (ROS). Structural characterization of Cu(II)/Cu(I) interaction is crucial to understand the possible role of copper toxicity in PD.
In this study, we investigated and compared the interaction of Cu(I) with the N-terminal portion of βS and αS by means of NMR, circular dichroism, and X-ray absorption spectroscopies.
This combined approach allowed us to (i) determine the Cu(I) coordination sphere, (ii) to understand the role of Met and His in metal binding and (iii) to obtain the structure of the metal complexes. The different Cu-Kα edges and XANES region of $\alpha S_{1\text{-}15}$ and $\beta S_{1\text{-}15}$ samples indicate the occurrence of different chemical environments for the two Cu(I) ions. In Figure 1, the superimposed experimental and simulated FT-EXAFS data are shown. Our data show the importance of M10K mutation occurring in βS, which induces different Cu(I) chemical environments(see Figure 1.1). Coordination modes 3S1O and 2S2O were identified for βS and αS, respectively. These new insights into the bioinorganic chemistry of copper and synuclein proteins are a basis to understand the molecular mechanism by which βS might inhibit αS aggregation.

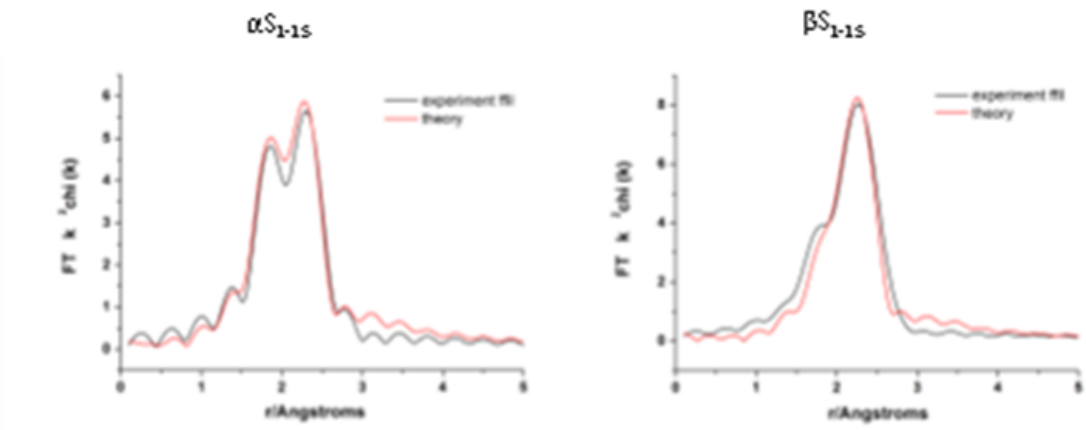

Figure 1, Comparison of the theoretical signal (red) with experimental data (black) of Fourier transforms of Cu K-edge XAS spectra of copper(I) complexes of $\alpha S_{1\text{-}15}$ and $\beta S_{1\text{-}15}$.

sample	R-factor	Atom type	Distance (Å)	Debye–Waller factor	N° shell
$\alpha S_{1\text{-}15}$ – Cu(I)	18.84	2O	1.924	0.0029	2
		2S	2.294	0.0055	
$\beta S_{1\text{-}15}$ – Cu(I)	22.48	O	1.950	0.0032	2
		3S	2.295	0.0073	

Publication: R. de Ricco et al., Inorg. Chem. 54 (2015), 4744.

1. Amendola V., Scaramuzza S., Agnoli S., Granozzi G., Meneghetti M., Campo G., Bonanni V., Pineider F., Sangregorio C., Ghigna P., Polizzi S., Riello P., Fiameni S., Nodari L. Laser generation of iron-doped silver nanotruffles with magnetic and plasmonic properties Nano Research ee 2015.
2. Benedetti F., Luches P., Spadaro M.C., Gasperi G., D'Addato S., Valeri S., Boscherini F. Structure and morphology of silver nanoparticles on the (111) surface of cerium oxide Journal of Physical Chemistry C 119 6024-6032 2015.
3. Caby B., Brigidi F., Ingerle D., Nolot E., Pepponi G., Streli C., Lutterotti L., André A., Rodríguez G., Gergaud P., Morales M., Chateigner D. Study of annealing-induced interdiffusion in In2O3/Ag/In2O3 structures by a combined X-ray reflectiv Spectrochimica Acta B 113 132 -137 2015 .
4. Centomo P., Meneghini C., Sterchele S., Trapananti A., Aquilanti G., Zecca M. EXAFS in situ: The effect of bromide on Pd during the catalytic direct synthesis of hydrogen peroxid Catalysis Today 248 138-141 2015
5. Centomo P., Meneghini C., Sterchele S., Trapananti A., Aquilanti G., Zecca M. In situ X-ray absorption fine structure spectroscopy of a palladium catalyst for the direct synthesi ChemCatChem 7 37123718 2015.
6. Cesca T., Kalinic B., Maurizio C., Scian C., Trave E., Battaglin G., Mazzoldi P., Mattei G. Correlation between room temperature luminescence and energy-transfer in ErAu co-implanted silica Nuclear Instruments and Methods in Physics Research B 362 68-71 2015.
7. Cesca T., Kalinic B., Michieli N., Maurizio C., Trapananti A., Scian C., Battaglin G., Mazzoldi P., Mattei G. AuAg nanoalloy molecule-like clusters for enhanced quantum efficiency emission of Er3+ions in silic Physical Chemistry - Chemical Physics 17 28262-28269 2015.
8. Cicconi M.R., Giuli G., Ertel-Ingrisch W., Paris E., Dingwell D.B. The effect of the [Na/(Na+K)] ratio on Fe speciation in phonolitic glasses American Mineralogist 100 1610-1619 2015.
9. De Ricco R., Valensin D., Dell'Acqua S., Casella L., Gaggelli E., Valensin G., Bubacco L., Mangani S. Differences in the binding of copper(I) to a- and ß-synuclein Inorganic Chemistry 54 265-272 2015.
10. Di Benedetto F., Cinotti S., Vizza F., Foresti M.L., Guerri A., Lavacchi A., Montegrossi G., Romanelli M., Cioffi N., Innocenti M. Electrodeposited semiconductors at room temperature: An X-ray absorption spectroscopy study of Cu-, Electrochimica Acta 179 495-503 2015.
11. Edla R., Patel N., Orlandi M., Bazzanella N., Bello V., Maurizio C., Mattei G., Mazzoldi P., Miotello A. Highly photo-catalytically active hierarchical 3D porous/urchin nanostructured Co3O4 coating synthes Applied Catalysis B: Environmental 166-167 475-484 2015.
12. Eiche E., Bardelli F., Nothstein A.K., Charlet L., Göttlicher J., Steininger R., Dhillon K.S., Sadana U.S. Selenium distribution and speciation in plant parts of wheat (Triticum aestivum) and Indian mustard Science of the Total Environment 505 952-961 2015.
13. Fornasini P., Grisenti R. On EXAFS debye-Waller factor and recent advances Journal of Synchrotron Radiation 22 1242-1257 2015.

14. Fornasini P., Grisenti R. On EXAFS debye-Waller factor and recent advances Journal of Synchrotron Radiation 22 1242-1257 2015.
15. Giuli G., Trapananti A., Mueller F., Bresser D., Passerini S. Insights into the effect of iron and cobalt doping on the structure of nanosized ZnO Inorganic Chemistry 54 9393-9400 2015.
16. Gualtieri M.L., Romagnoli M., Pollastri S., Gualtieri A.F. Inorganic polymers from laterite using activation with phosphoric acid and alkaline sodium silicate Cement and Concrete Research 67 259-270 2015.
17. Haubold E. Strukturanalyse kupferarmer Cu-(In,Ga)-Se Phasen mittels Röntgenabsorptionsspektroskopie (Structural 2015.
18. Maurizio C., Cesca T., Kalinic B., Trapananti A., Scian C., Battaglin G., Mazzoldi P., Mattei G. Gold-based nucleation in implanted silica studied by x-ray absorption spectroscopy Ceramics International 41 8660-8664 2015.
19. Maurizio C., Checchetto R., Trapananti A., Rizzo A., Miotello A. In situ X-ray absorption spectroscopy-X-ray diffraction investigation of Nb-H nanoclusters in MgH2 d Journal of Physical Chemistry C 119 7765-7770 2015.
20. Minguzzi A., Locatelli C., Lugaresi O., Achilli E., Cappelletti G., Scavini M., Coduri M., Masala P., Sacchi B., Vertova A., Ghigna P., Rondinini S. Easy accommodation of different oxidation states in iridium oxide nanoparticles with different hydra ACS Catalysis 5 5104-5115 2015.
21. Pethes I., Chahal R., Nazabal V., Prestipino C., Trapananti A., Pantalei C., Beuneu B., Bureau B., Jóvári P. Short range order in Ge-Ga-Se glasses Journal of Alloys and Compounds 651 578-584 2015.
22. Pollastri S., d'Acapito F., Trapananti A., Colantoni I., Andreozzi G.B., Gualtieri A.F. The chemical environment of iron in mineral fibres. A combined X-ray absorption and Mössbauer spectr Journal of Hazardous Materials 298 282-293 2015.
23. Souchier E., d'Acapito F., Noé P., Blaise P., Bernard M., Jousseaume V. The role of the local chemical environment of Ag on the resistive switching mechanism of conductive Physical Chemistry - Chemical Physics 17 23931-23937 2015.
24. Torrengo S., Paul M.C., Halder A., Das S., Dhar A., Sahu J.K., Jain S., Kir'yanov A.V., d'Acapito F. EXAFS studies of the local structure of bismuth centers in multicomponent silica glass based optical Journal of Non-Crystalline Solids 410 82-87 2015.
25. Ventruti G., Della Ventura G., Scordari F., Susta U., Gualtieri A.F. In situ high-temperature XRD and FTIR investigation of hohmannite, a water-rich Fe-sulfate, and its Journal of Thermal Analysis and Calorimetry 119 1793-1802 2015.
26. Wang L., Lavacchi A., Bellini M., Di Benedetto F., Innocenti M., Miller H.A., Montegrossi G., Zafferoni C., Vizza F. Deactivation of palladium electrocatalysts for alcohols oxidation in basic electrolytes Electrochimica Acta 177 100-106 2015.

Contacts

Beamline responsible:	Francesco d'Acapito dacapito@esrf.fr +33 4 7688 2426 , +33 6 8936 4302
Beamline scientists:	Alessandro Puri puri@esrf.fr +33 4 7688 2859
	Giovanni Lepore lepore@esrf.fr +33 4 7688 2530
Local Contact:	+33 6 8838 6994
Beamline:	+33 4 7688 2085
Laboratory:	+33 4 7688 2743
Skype:	gilda_beamline
Administration:	Fabrizio La Manna lamanna@esrf.fr +33 4 7688 2962
Web page:	http://www.esrf.eu/UsersAndScience/Experiments/CRG/BM08/

Forthcoming proposals submission deadlines

CRG quota: May, 8th, Nov. 8th 2016

ESRF quota: March 1st, Sept 10th 2016

Contributors to this issue

F. d'Acapito, A. Puri, G. Lepore (CNR-IOM, Grenoble)

R. De Donatis (CNR, Genova)

G. Giuli (Univ. Camerino)

A. Minguzzi (Univ. Milano)

P. Ghigna, M. Fracchia (Univ. Pavia)

M. R. Cicconi (Univ. Erlangen-Nürnberg)

A. Pollastri (Univ. Modena)

P. Luches (UNiv. Modena)

S. Mangani (Univ. Siena)